Strong magnetic x-ray dichroism in 2p absorption spectra of 3d transition-metal ions

G. van der Laan

SERC Daresbury Laboratory, Warrington WA4 4AD, United Kingdom

B. T. Thole

*Materials Science Center, University of Groningen, Nijenborgh 16, 9747 AG Groningen,
The Netherlands*

(Received 10 September 1990)

From atomic calculations in crystal-field symmetry we find a very strong circular and linear dichroism in the $2p$ x-ray absorption edges of magnetically ordered $3d$ transition-metal ions. The spectral shape changes drastically with the character of the ground state, which is determined by the presence of a crystal field, and the relative magnitudes of the exchange and $3d$ spin-orbit interaction. The difference in integrated intensity of the $2p$ absorption for left- and right-circular polarization provides a measure for the $3d$ spin-orbit coupling in spherical and crystal-field symmetry. The anisotropic branching ratio depends on the spin-orbit interaction and the Van Vleck contribution of the exchange interaction. The results of our calculations provide a basis for the study of magnetic x-ray dichroism on materials with localized $3d$ electrons.

I. INTRODUCTION

Synchrotron radiation has become an important tool for the study of the electronic structure of solids. The advent of devices which offer highly polarized synchrotron radiation has made it possible to investigate also the magnetic structure. Analysis of the magnetic structure which used x-rays was initially based on diffraction. In 1970 Platzman and Tzoar[1] indicated that a magnetically ordered material gives a small spin-dependent contribution to the x-ray scattering cross section. This magnetic diffraction was observed in 1972 by deBergevin and Brunel[2] in antiferromagnetic NiO, where magnetic superlattice reflections are decoupled from the structural Bragg peaks. The orbital and spin momentum can be separated due to the different Bragg-angle dependence in x-ray diffraction, which gives an advantage over neutron diffraction.[3] In ferromagnet and ferrimagnets the charge and magnetic Bragg peaks coincide, but there is a large enhancement of the scattering cross section at the absorption edge due to the interference term between the imaginary part of the charge structure factor and the magnetic structure factor.[4]

X-ray scattering gives information about the structure of the magnetic lattice. Instead, x-ray absorption spectroscopy (XAS) can be used as an element- and site-selective probe to study the unoccupied electronic density of states. The possibility of assessing the local magnetic moment with XAS is much less explored. In 1974 Erskine and Stern[5] predicted a magneto-optical effect in the $3p$ absorption edge of ferromagnetic nickel from augmented-plane-wave (APW) calculations. The spin-orbit splitting of the $3p$ core level in combination with the $3d$ final-state spin polarization results in a magneto-optical Kerr effect (MOKE) of $\sim 10\%$. An attempt to observe MOKE in the Gd $2p \rightarrow 5d$ transition of amorphous Gd-Fe alloy gave an upper limit of 0.02%.[6] These

were the only reports on magnetic dichroism until in 1985 Thole, van der Laan, and Sawatzky[7] predicted a strong magnetic x-ray dichroism (MXD) in the $3d$ absorption edges of rare-earth materials on the basis of atomic multiplet calculations. It was suggested that complicated magnetic structures can be studied using *circular and linear* polarizations, which give the average value of $\langle M \rangle$ and $\langle M^2 \rangle$ of the local magnetization, respectively. This has been demonstrated experimentally on terbium iron garnet.[8] As an interesting application Goedkoop et al.[9] proposed to exploit this effect to change linearly polarized synchrotron radiation into circularly polarized radiation by using a magnetic transmission foil. Spin-dependent effects, which were confirmed by first-principles calculations,[10] have also been reported in rare-earth L edges and transition-metal K edges.[11−13] For these core levels Carra and Altarelli[14] pointed out the contribution of electrical quadrupole transitions. At present, magnetic dichroism is under development by various groups in major synchrotron facilities with the emphasis on the $1s$ edges of $3d$ transition metals, the $2p$ edges of $4d$ and $5d$ transition metals, and the $2p$ and $3d$ edges of the rare earths.[15]

The $2p$ edges of $3d$ transition metals are less studied, because the energy region between 400 and 800 eV is difficult to cover, both with grating and double crystal monochromators. However, the $2p$ edges have several specific advantages: (a) the core-hole lifetime broadening is only 100 to 300 meV, resulting in sharp multiplet structures, (b) the $2p_{3/2}$ and $2p_{1/2}$ spectral parts are clearly separated, and (c) the dipole transition excites the $2p$ electron into the localized $3d$ shell, which has the magnetic moment. Recently, Chen and Sette have constructed a spherical grating monochromator with a strongly improved energy resolution in the soft-x-ray region[16] and observed MXD in the Co $2p$ edge of $BaCoF_4$,[17] and in the $2p$ edge of the ferromagnetic metals,[18] ferrites, and gar-

nets.[19] However, the circularly polarized branching ratio in nickel was found to differ appreciably from that predicted by the exchange-split-valence-band model of Erskine and Stern.[5]

In the $3d$ transition-metal compounds the one-electron model is not a good approximation because of the localized character of the $3d$ electrons.[20] An atomic approach including crystal- or ligand-field interaction gives an excellent agreement with experimental isotropic x-ray absorption spectra as has been shown by several calculations of $3d$ transition-metal ions.[21-25] Furthermore, the $2p$ branching ratio, which cannot be explained by one-electron theory, can be derived from atomic calculations.[26] It is expected that atomic calculations can also give accurate MXD spectra which are determined by angular momentum coupling. This has already been shown for rare-earth materials, where the magnetic interaction can be treated as a perturbation.[8,27] In the case of the $3d$ metals, however, the ground and excited states have to be calculated in the presence of spin-orbit, electrostatic, and exchange interactions that cannot be treated as small perturbations.

In this paper we will present results of atomic and crystal-field calculations for magnetically ordered $3d$ transition-metal ions. We will give spectra for two separate cases: the spin-orbit splitting equal to the atomic value, and equal to zero. This paper is organized as follows. Section II describes the theory. Section III explains the method of calculation. Section IV shows the calculated spectra, which are discussed in Sec. V. Because of their importance, the intensity and branching ratio are discussed separately in Secs. VI and VII. Finally, conclusions are derived in Sec. VIII.

II. THEORY

The $2p$ absorption in $3d$ transition-metal ions can be obtained from the dipole transition probability $3d^n \rightarrow 2p^5 3d^{n+1}$. Quadrupole transitions play no role in this excitation. In the spherically symmetric potential of a free ion a small $3d$ spin-orbit interaction will split the initial state LS terms into levels LSJ. These levels are $(2J+1)$-fold degenerate, corresponding to the number of distinct eigenvalues $M_J = -J, -J+1, \ldots, J$. The electrons are coupled to those of neighboring atoms by exchange interactions among which we can distinguish direct-exchange, indirect-exchange, itinerant-exchange and superexchange. Indirect- and itinerant-exchange (in the order of a few eV) occur in metallic systems, which are not considered here. Direct exchange and superexchange, which are important mechanisms in nonmetallic systems, are usually between 0.005 and 0.1 eV.[28,29] The interatomic exchange interaction in the $3d$ metal compounds can be treated as a magnetic field acting only on the spin S. This exchange field lifts the degeneracy, making the energy of the M_J sublevels equal to $-g\mu_B H M_J$, where only the level with $M_J = -J$ is populated at $T=0$ K. The factor g depends on the values of L, S, and J. If the exchange interaction is of the same order of magnitude as the spin-orbit interaction, the different J levels within the term are strongly mixed. The energy of the

final-state levels J' is determined by the electrostatic interactions in the $2p^5 3d^{n+1}$ configuration and the large core-hole spin-orbit interactions, which splits the spectrum into a $2p_{3/2}$ and a $2p_{1/2}$ parts.

Magnetic dichroism is induced by the optical selection rules. This can be easily seen in the case that the spin-orbit splitting in the initial state is large, so that J is a good quantum number. In the final state J' is a good quantum number due to the large core hole spin-orbit interaction. From a given initial-state level J, the dipole selection rule $\Delta J = +1, 0, -1$ permits only transitions to final-state levels $J' = J+1$, J, and $J-1$. Excitation with left-circularly polarized radiation ($\Delta M_J = -1$) is then only allowed to $J' = J+1$ levels, the only levels which contain an $M_{J'} = -M_J - 1$ sublevel. Excitation with right-circularly polarized radiation ($\Delta M_J = +1$) is allowed to all $J' = J+1, J$, and $J-1$ levels, since they all contain an $M_{J'} = -M_J + 1$ sublevel. The levels with different total angular momentum J' in the final-state configuration $2p^5 3d^{n+1}$ have a different energy distribution due to the electrostatic interactions between the $2p$ core-hole and $3d$ valence electrons, and the $2p$ core-hole spin-orbit interaction. Therefore, the spectra for left- and right-circularly polarized radiation will be different. The transition probabilities are given by the Wigner-Eckart theorem, which can also be used to describe the temperature dependence of the spectra.[7] The dichroic effect is strongest at $T=0$ K and gradually reduces when higher magnetic sublevels are populated.

In the presence of crystal-field interaction or large exchange interaction, J ceases to be a good quantum number and the selection rules are more complicated, barring the use of the simple model where the magnetic interaction is treated as a perturbation using the Wigner-Eckart theorem. Instead, calculations have to be performed in intermediate coupling, taking all interactions into account.

III. CALCULATIONAL DETAILS

Calculations were performed using the chain of groups approach exposed by Butler.[30] This approach starts with the calculation of the reduced matrix elements of the necessary operators in the spherical group using Cowan's atomic multiplet program.[31] The Wigner-Eckart

TABLE I. The *ab initio* values (in eV) of the parameters in the Hartree-Fock calculation for the initial-state configurations. The actual values for the Coulomb and exchange interaction used in the calculation have been scaled to 80% of these values.

Configuration	$F^2(d,d)$	$F^4(d,d)$	$\zeta(3d)$
V^{4+} d^1			0.031
V^{3+} d^2	10.127	6.354	0.027
Cr^{3+} d^3	10.777	6.755	0.035
Cr^{2+} d^4	9.649	6.002	0.030
Mn^{2+} d^5	10.316	6.414	0.040
Fe^{2+} d^6	10.966	6.815	0.052
Co^{2+} d^7	11.605	7.209	0.066
Ni^{2+} d^8	12.234	7.598	0.083

TABLE II. The character of the ground state for the d^n configurations in spherical [O(3)] and octahedral (O_h) symmetry.

Configuration	O(3)	O_h (high spin)	O_h (low spin)
V^{4+} d^1	$^2D_{3/2}$	$(t_2^1, {}^2T_2)$ U'	
V^{3+} d^2	$^3F_2$	$(t_2^2, {}^3T_1)$ E	
Cr^{3+} d^3	$^4F_{3/2}$	$(t_2^3, {}^4A_2)$ U'	
Cr^{2+} d^4	$^5D_0$	$(t_2^3e^1, {}^5E)$ A_1	$(t_2^4, {}^3T_1)$ A_1
Mn^{2+} d^5	$^6S_{5/2}$	$(t_2^3e^2, {}^6A_1)$ U',E'	$(t_2^5, {}^2T_2)$ E''
Fe^{2+} d^6	$^5D_4$	$(t_2^4e^2, {}^5T_2)$ T_2	$(t_2^6, {}^1A_1)$ A_1
Co^{2+} d^7	$^4F_{9/2}$	$(t_2^5e^2, {}^4T_1)$ E'	$(t_2^6e^1, {}^2E)$ U'
Ni^{2+} d^8	$^3F_4$	$(t_2^6e^2, {}^3A_2)$ T_2	

theorem is applied to obtain the reduced matrix elements in the desired point group, where the required isoscalar factors are obtained from Butler's point-group program.[30]

The initial state $3d^n$ in the free ion is split by the Coulomb interactions $F^{2,4}(d,d)$ and the spin-orbit interaction $\zeta(3d)$. The ab initio values of these interactions are given in Table I for each configuration. Table II gives the irreducible representations of the ground state in the spherical symmetry O(3) and octahedral symmetry O_h. The final-state configuration $2p^53d^{n+1}$ is split by spin-orbit and electrostatic interactions. The ab initio values of the involved parameters $\zeta(2p)$, $\zeta(3d)$, $F^{2,4}(d,d)$, $F^2(p,d)$ and $G^{1,3}(p,d)$ are given in Table III. In the actual calculation of the initial and final states the Slater integrals have been scaled down to 80% of the atomic values to account for intra-atomic relaxation effects. The F^0 term, which contributes only to the average energy, is not tabulated.

The crystal field reduces the spherical symmetry O(3) to octahedral symmetry O_h and the irreducible representations LSJ are projected onto representations $\Gamma S \Gamma_J$ of the lower group, where Γ_J is the total symmetry. A magnetic field along the z axis reduces the symmetry from O_h to C_4 and lifts the Kramers degeneracy. The exchange field is included by a term $g\mu_B HS$ in the Hamiltonian with $\mu_B H = 0.01$ eV. The representation for the dipole operator ($J=1$) is threefold degenerate in cubic symmetry and splits in C_4 symmetry into $q = -1, 0, +1$ which correspond to left-circularly, z-, and right-circularly polarized radiation, respectively.

The core-hole lifetime is taken into account by a convolution of the $2p_{3/2}(2p_{1/2})$ lines with a Lorentzian of 0.1 (0.3) eV and the experimental broadening by a Gaussian of $\sigma = 0.15$ eV.

IV. RESULTS

For brevity, we have introduced some obvious notations. The spectra excited with isotropic, x-, y-, z-, and left- and right-circularly polarized radiation are called the I, X, Y, Z, L, and R spectra, respectively. For these spectra we have $I = (L+Z+R)/3$ and $X = Y = (L+R)/2$. The sensitivity for circularly and linearly polarized radiation is contained in the $L-R$ and $Z-X$ spectra, respectively. Figure 1 shows the calculated $I, L, Z, R, L-R$, and $Z-X$ spectra for the ground-state configurations, given in Table II. The different panels represent the O(3) symmetry and the O_h symmetry ($10Dq = 1$, 2, and 3 eV) with the scaling factor z for the 3d spin-orbit parameter equal to 1 (top row) or 0 (bottom row). For $z = 1$, the spin-orbit parameter has the atomic Hartree-Fock value (Table I) and the ground state has the character of the lowest (O(3))LSJ or (O_h)$\Gamma S \Gamma_J$ level.

TABLE III. The ab initio values (in eV) of the parameters in the Hartree-Fock calculation for the final state configurations. The actual values for the Coulomb and exchange interaction used in the calculation have been scaled to 80% of these values.

Configuration	$F^2(d,d)$	$F^4(d,d)$	$F^2(p,d)$	$G^1(p,d)$	$G^3(p,d)$	$\zeta(2p)$	$\zeta(3d)$
V^{4+} p^5d^2	11.965	7.554	6.759	5.014	2.853	4.650	0.042
V^{3+} p^5d^3	10.974	6.888	6.057	4.392	2.496	4.649	0.036
Cr^{3+} p^5d^4	11.596	7.270	6.526	4.788	2.722	5.667	0.047
Cr^{2+} p^5d^5	10.522	6.552	5.841	4.024	2.388	5.668	0.041
Mn^{2+} p^5d^6	11.155	6.943	6.321	4.606	2.618	6.846	0.053
Fe^{2+} p^5d^7	11.779	7.327	6.793	5.004	2.844	8.200	0.067
Co^{2+} p^5d^8	12.396	7.708	7.260	5.397	3.069	9.746	0.083
Ni^{2+} p^5d^9			7.721	5.787	3.291	11.507	0.102

The mixing of excited levels into the ground state, the so called van Vleck contribution, has been included. We have taken an initial state summed over all levels within 10^{-4} eV from the ground state, which corresponds to $T \approx 1$ K. For $z = 0$, the initial state is the weighted average over all spin-orbit levels $(O(3))LSJ$ or $(O_h)\Gamma S\Gamma_J$ in

the ground-state term $(O(3))LS$ or $(O_h)\Gamma S$. The spectra show a temperature dependence, because the spin-orbit and exchange interaction are both in the order of kT. When all spin-orbit split levels of the ground state term are equally populated we obtain the $z = 0$ spectrum. When the magnetic sublevels are equally populated we

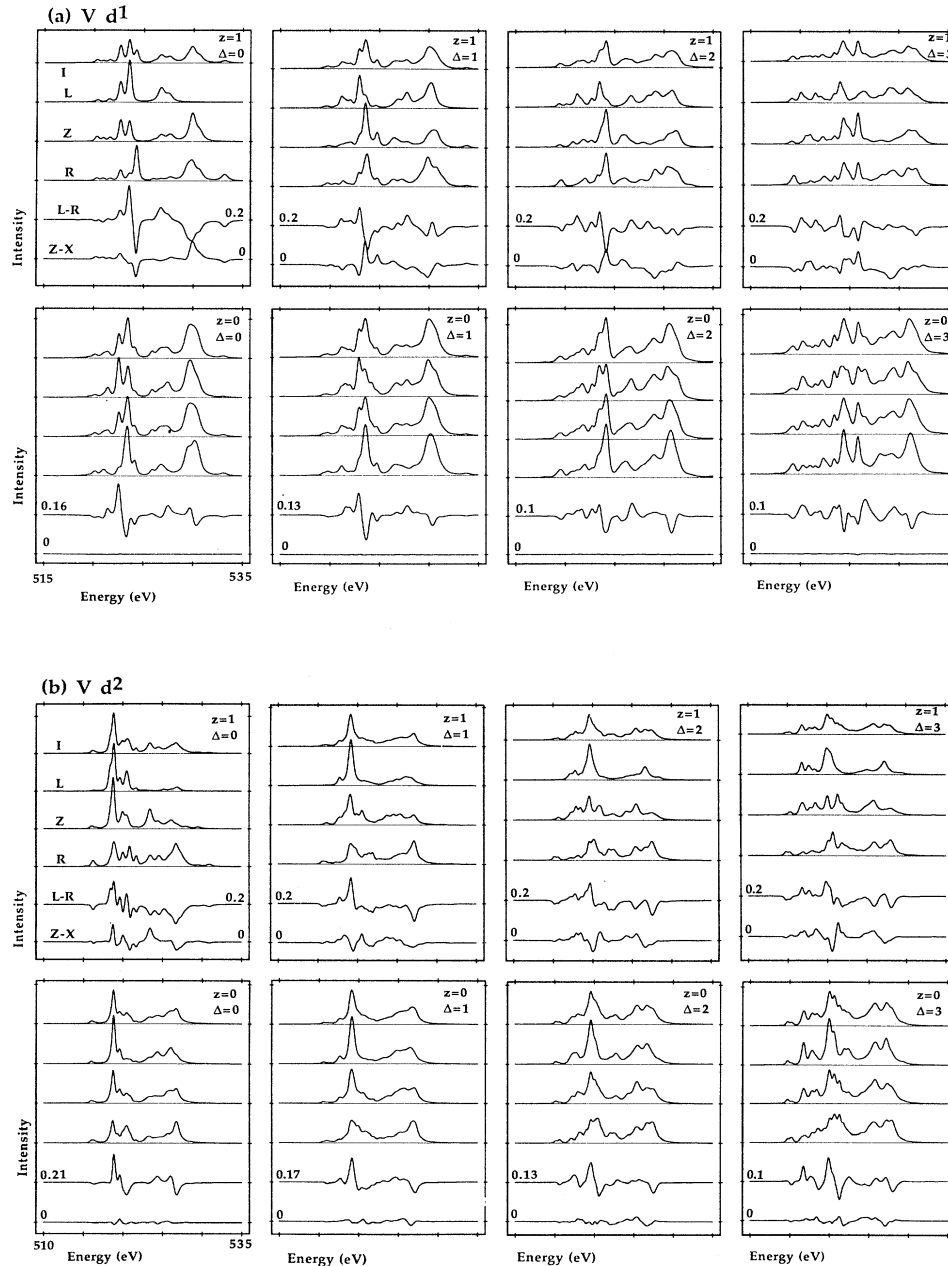
FIG. 1. The transition probability $3d^n \rightarrow 2p^53d^{n+1}$ in the presence of an exchange field. The Slater integrals and spin-orbit parameters are 80% and 100% of the atomic values, respectively, and the exchange interaction is 0.01 eV. The information for each ion of Table II is contained in a set of eight panels. In the upper (lower) row of four panels the scaling factor z of the $3d$ spin-orbit interaction is equal to 1 (0). From left to right, the columns of panels are for $\Delta = 10Dq = 0$, 1, 2, and 3 eV in O_h symmetry [$\Delta = 10Dq = 0$ eV is equivalent to $O(3)$ symmetry]. From top to bottom the six curves inside each panel give the isotropic (I), left-circularly (L), $z - (Z)$, right-circularly R polarized spectrum and the $L - R$ and $Z - X$ difference spectrum. The numbers near the bottom give the intensity scale for each panel.

obtain the isotropic spectrum.

Ions with the same number of $3d$ electrons give similar spectra, except for the size of $2p$ spin-orbit separation and the absolute energy. Only one element for each d count has been given, where we have chosen for naturally abundant ions. The isoelectronic Ti^{3+} can be obtained from V^{4+}, Mn^{4+} from Cr^{3+}, Mn^{3+} from Cr^{2+}, Fe^{3+} from Mn^{2+} and Co^{3+} from Fe^{2+}.

The integrated intensity P and branching ratio B of each spectrum is given in Table IV. We found only minor changes in P and B as a function of $10Dq$ for constant values of z and $2S+1$. This makes it possible to give characteristic values of P and B for each type of ground state, independent of $10Dq$. This cannot be done for Ni d^8, where the large second-order spin-orbit interaction gives a contribution to the isotropic branching ratio, which is proportional to $\zeta(3d)/10Dq$.[26] The systematic trends in the intensity and the branching ratio are discussed in Secs. VI and VII, respectively.
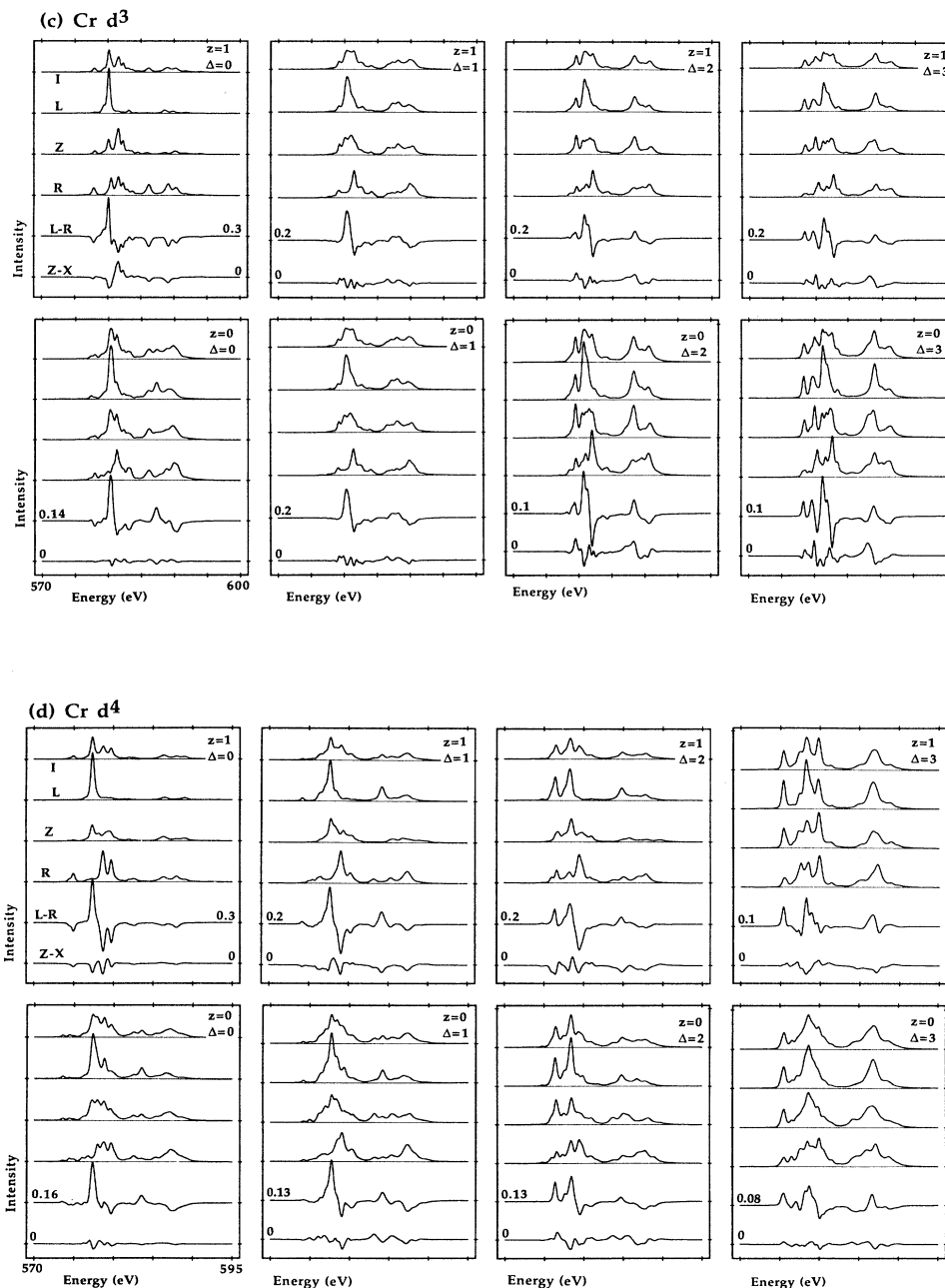

(c) Cr d^3

(d) Cr d^4

FIG. 1. (Continued).

V. DISCUSSION

A. General

All states give circular magnetic dichroism, except the singlet state, $d^6\,{}^1A_1$, which does not split by exchange interaction. Doublet states without spin-orbit interaction, $d^1\,{}^2D$, $d^1\,{}^2T_2$, $d^5\,{}^2T_2$, and $d^7\,{}^2E$, show no linear polarization. This can be understood as follows. The ground-state spin is split into only two levels: a Kramer's pair.

The final state is also split but this splitting is smaller than the core-hole lifetime width and is not detectable. These final-state levels can therefore be considered as degenerate. Suppose that the ground state is split into ψ_1 and ψ_2, where $\psi_2 = \psi_1^*$ and some final-state contains the degenerate pair $\psi_{f2} = \psi_{f1}^*$, then

$$\langle \psi_1 | z | \psi_{f1} \rangle = \langle \psi_2 | z | \psi_{f2} \rangle^* \ . \tag{1}$$

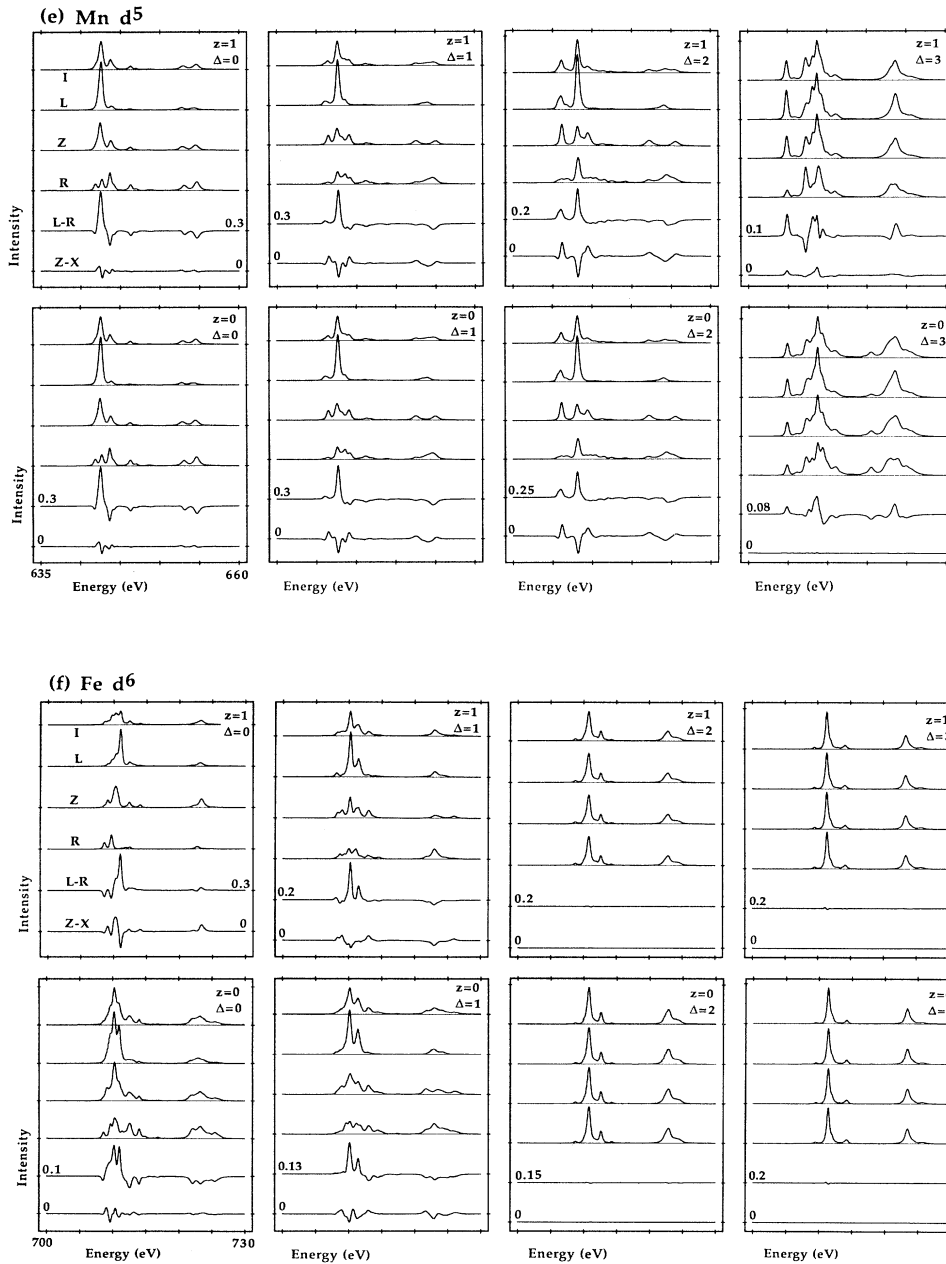Therefore, the spectrum of ψ_1 is equal to that of ψ_2 and

FIG. 1. (*Continued*).

the spectrum of the doublet state is the same as that of the unsplit state, which was isotropic. Figure 1 shows that for the other spin states the linear dichroism is in general smaller than the circular dichroism.

There is a large difference between the $z=0$ and 1 spectra when there is first-order spin-orbit splitting, which occurs for ground-state terms with orbital degeneracy and $S\neq 0$, except the (two-dimensional) E representation. Thus, there is first-order splitting for d^1, d^2, low-spin d^4 and d^5, high-spin d^6 and d^7 in O_h, and for all configurations in O(3) symmetry, except d^5.

The spectra—given here for an exchange interaction of 0.01 eV—are strongly dependent on the relative magnitude of the exchange interaction and the spin-orbit split-
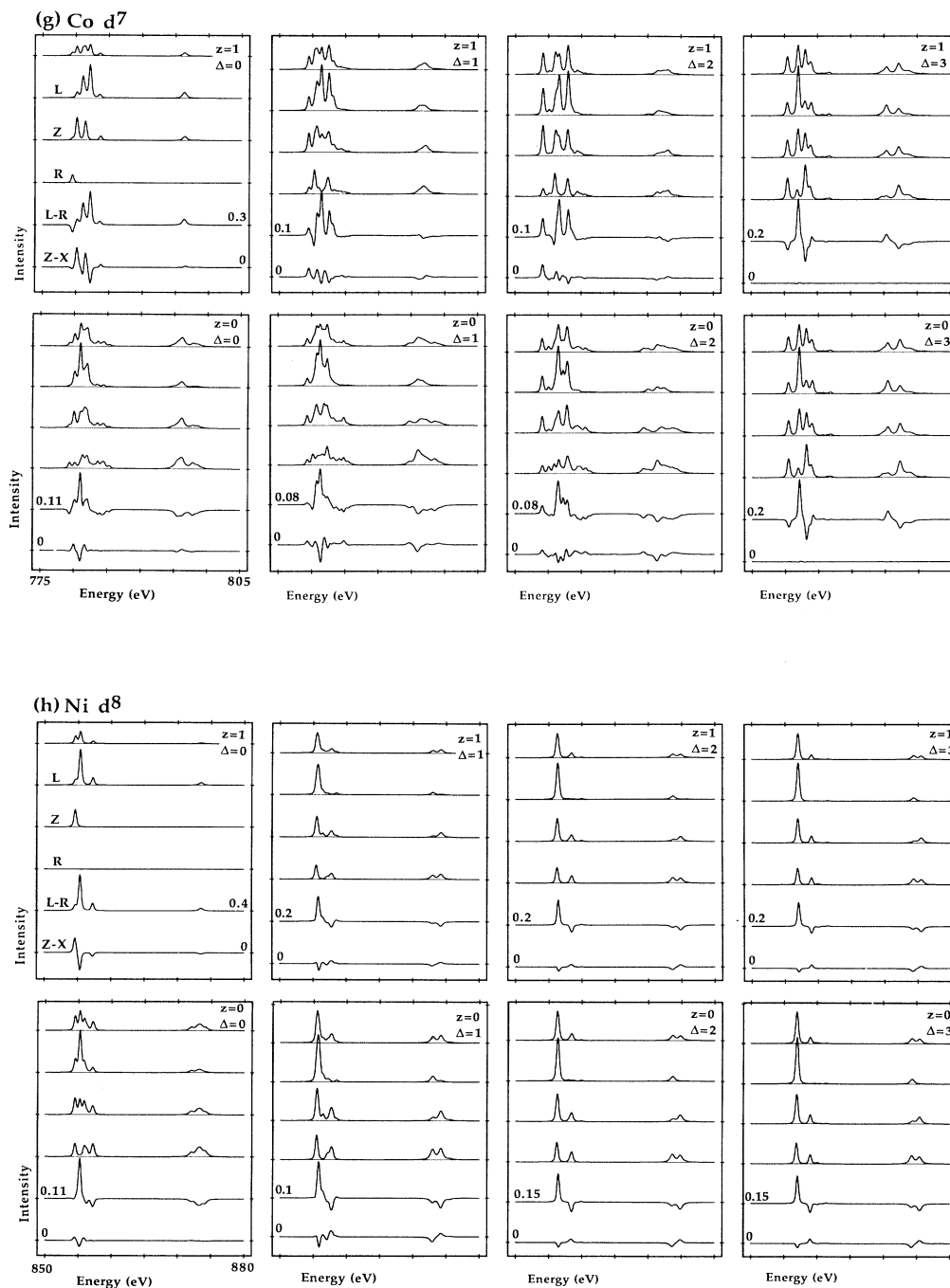

FIG. 1. (Continued).

G. van der LAAN AND B. T. THOLE

TABLE IV. The integrated intensity P and the branching ratio B of the $2p$ absorption spectra for isotropic, left-circularly, z-, and right-circularly polarized radiation.

Configuration	Ground state	$P(i)$	$P(l)$	$P(z)$	$P(r)$	$B(i)$	$B(l)$	$B(z)$	$B(r)$
V d^1	$^2D_{3/2}$	0.60	0.48	0.65	0.67	0.46	0.63	0.38	0.41
	$(^2T_2)\ U'$	0.60	0.57	0.57	0.67	0.42	0.39	0.48	0.39
	$^2D,\ ^2T_2;\ z=0$	0.60	0.60	0.60	0.60	0.40	0.40	0.40	0.40
V d^2	$^3F_2$	0.53	0.38	0.56	0.66	0.58	0.88	0.56	0.43
	$(^3T_1)\ E$	0.53	0.45	0.56	0.59	0.52	0.63	0.52	0.40
	$^3F,\ ^3T_1;\ z=0$	0.53	0.53	0.53	0.53	0.47	0.49	0.47	0.46
Cr d^3	$^4F_{3/2}$	0.47	0.34	0.44	0.62	0.69	0.83	0.80	0.54
	$(^4A_2)\ U'$	0.47	0.46	0.47	0.47	0.56	0.62	0.54	0.53
	$^4F,\ ^4A_2;\ z=0$	0.47	0.47	0.47	0.47	0.55	0.58	0.55	0.52
Cr d^4	$^5D_0$	0.40	0.33	0.35	0.52	0.76	0.86	0.73	0.72
	$(^5E)\ A_1$	0.40	0.43	0.33	0.44	0.65	0.62	0.72	0.63
	$(^3T_1)\ A_1$	0.40	0.45	0.38	0.37	0.63	0.63	0.67	0.59
	$^5D,\ ^5E;\ z=0$	0.40	0.40	0.40	0.40	0.63	0.70	0.63	0.56
	$^3T_1;\ z=0$	0.40	0.40	0.40	0.40	0.57	0.61	0.56	0.53
Mn d^5	$^6S_{5/2}$	0.33	0.33	0.33	0.33	0.76	0.87	0.75	0.65
	$(^6A_1)\ U',E'$	0.33	0.33	0.33	0.33	0.76	0.87	0.76	0.65
	$(^2T_2)\ E''$	0.33	0.38	0.34	0.28	0.69	0.69	0.69	0.67
	$^6S,\ ^6A_1;\ z=0$	0.33	0.33	0.33	0.33	0.75	0.87	0.75	0.64
	$^2T_2;\ z=0$	0.33	0.33	0.33	0.33	0.59	0.62	0.59	0.57
Fe d^6	$^5D_4$	0.27	0.33	0.33	0.13	0.80	0.86	0.73	0.81
	$(^5T_2)\ T_2$	0.27	0.32	0.25	0.23	0.78	0.85	0.83	0.61
	$(^1A_1)\ A_1$	0.27	0.27	0.27	0.27	0.63	0.63	0.63	0.63
	$^5D,\ ^5T_2;\ z=0$	0.27	0.27	0.27	0.27	0.72	0.86	0.72	0.59
	$^1A_1;\ z=0$	0.27	0.27	0.27	0.27	0.60	0.60	0.60	0.60
Co d^7	$^4F_{9/2}$	0.20	0.33	0.23	0.03	0.86	0.86	0.86	1.00
	$(^4T_1)\ E'$	0.20	0.25	0.21	0.14	0.83	0.88	0.85	0.72
	$(^2E)\ U'$	0.20	0.20	0.20	0.20	0.67	0.72	0.67	0.63
	$^4F,\ ^4T_1;\ z=0$	0.20	0.20	0.20	0.20	0.71	0.85	0.70	0.57
	$^2E;\ z=0$	0.20	0.20	0.20	0.20	0.63	0.67	0.63	0.58
Ni d^8	$^3F_4$	0.13	0.30	0.10	0.00	0.93	0.91	1.00	
	$(^3A_2)\ T_2\ (10Dq=1\ \text{eV})$	0.13	0.15	0.13	0.12	0.75	0.88	0.75	0.58
	$(^3A_2)\ T_2\ (10Dq=3\ \text{eV})$	0.13	0.14	0.13	0.13	0.71	0.85	0.72	0.55
	$^3F,\ ^3A_2;\ z=0$	0.13	0.13	0.13	0.13	0.69	0.84	0.69	0.54

ting. The exchange interaction mixes higher J levels into the ground-state level, especially those levels which originate from the same LS term. These effects are clearly seen for the $d^4\,^5D_0$ ground state, which has no dichroism in the absence of J mixing. The $3d$ spin-orbit interaction results in a J manifold for the ^5D term with an energy spread of 0.076 eV. The circular dichroism has the same order of magnitude as the isotropic intensity if the exchange interaction is larger than 10^{-3} eV. For $\mu_B H = 10^{-4}$ eV, the circular dichroism reduces to 2% of the spectrum. Thus, the absolute intensity of the L-R spectrum depends strongly on the ratio of the exchange and $3d$ spin-orbit interaction. However, the shape of the L-R spectrum is independent of this ratio, since the same wave functions are mixed into the ground state. Di-

chroism is an extremely sensitive effect which already appears for magnetic interactions in the order of 1 K. For $\mu_B H = 10^{-2}$ eV there are small shoulders in the isotropic spectrum which are due to mixing with higher J levels. These features disappear in the absence of a magnetic field. The action of the exchange field can be compared with that of a crystal field. If its strength is in the order of the $3d$ spin-orbit interaction or the Coulomb interactions, the character of the ground state and, hence, the isotropic spectrum, may change drastically. In the case of Cr d^4 we find that the branching ratio of the spectra does not depend on the magnitude of the exchange interaction. In general, the branching ratio decreases when the exchange interaction mixes higher J levels into the ground state.

It is interesting to make a comparison with the $3d$ spectra of the rare earths which can also be obtained using atomic calculations. In these $3d$ edges one observes an $L-R$ spectrum which looks like a dispersion curve that goes from positive to negative with increasing energy.[32] This has been explained[33] using the Wigner-Eckart theorem, which gives the relation between the $\Delta J=+1$, 0, and -1 contributions and the L, Z, and R spectra. The absorption spectrum is bunched into three contributions $\Delta J=+1$, 0, and -1, where the $\Delta J=+1$ transitions have on average a lower energy than the $\Delta J=-1$ transitions due to the large electrostatic interaction between the $3d$ core hole and the $4f$ electrons in the rare earths. This causes the peculiar shape of the rare-earth spectra. In the $3d$ transition metals this shape is not so characteristic, because the separate contributions are too broad to be clearly distinguishable.

B. Configurations in detail

d^1: In O_h symmetry the first-order spin-orbit interaction splits the $^2T_2$ ground state into U' and E'' levels, which have different spectra and branching ratios. The sum over these levels is given by the $z=0$ spectrum. The d^1 doublet state without spin-orbit splitting has no linear dichroism, as a result of Eq. (1).

d^2: In O_h symmetry the first-order spin-orbit interaction splits the $^3T_1$ state into E, T_2, T_1, and A_1 levels with different spectra and branching ratios.

d^3: The spectra $z=0$ and 1 are very similar in O_h symmetry. This is because there is no first-order spin-orbit splitting of the $^4A_2$ term and second-order effects are small because the excited U' levels are far away.

d^4: The strong dichroism in O(3) symmetry is due to the large J mixing in the ground state as discussed in Sec. V A. The ^5E state in O_h symmetry contains the levels A_1, T_1, E, T_2, and A_2, which are almost degenerate, because the ^5E state does not split in first order. At moderate temperature these levels have to be summed, which will give the $z=0$ spectrum. The high-spin to low-spin transition occurs for a value of $10Dq$ between 2 and 3 eV. The first-order spin-orbit interaction splits the low-spin $^3T_1$ into A_1, T_1, E, and T_2, which have different spectra.

d^5: In O_h symmetry there is no first-order spin-orbit splitting in the high-spin $^6A_1$ state: the spectra of $z=0$ and 1 are very similar. The high-spin to low-spin transition occurs for a value of $10Dq$ between 2 and 3 eV. The low-spin doublet state $^2T_2$ has no linear polarization for $z=0$. First-order spin-orbit interaction splits this state into U' and E'', which give different spectra.

d^6: First-order spin-orbit interaction splits the high-spin $^5T_2$ state into T_2, E, T_1, A_1, T_1, and T_2 levels, which give different spectra and branching ratios. The high-spin to low-spin transition occurs for a value of $10Dq$ between 1 and 2 eV. The low-spin state $^1A_1$, which does not split by exchange interaction, has neither linear nor circular polarization dependence.

d^7: First-order spin-orbit interaction splits the high-spin $^4T_1$ state into E', U', U', and E'' levels, which have different spectra. The high-spin to low-spin transition

occurs for a value of $10Dq$ between 2 and 3 eV. The spectral shapes of the low-spin $(^2E)U'$ state for $z=0$ and 1 (averaged over the two lowest levels) are similar, but the branching ratios are different. The low-spin doublet state, which is four-fold degenerate, has no linear polarization for $z=0$. Also, the $z=1$ spectrum shows no linear polarization because we have averaged over the two lowest levels with an energy separation of 8×10^{-5} eV. The spectrum of the lowest energy level is distinctly different and does show a linear polarization dependence.

d^8: The $^3A_2$ is not split by first order spin-orbit interaction. The second order interaction with the excited T_2 level gives a strong dependence of the branching ratio on the spin-orbit interaction.[26]

d^9: The results for Cu^{2+} have been discussed in an earlier paper,[34] where an analytical expression was given for the temperature dependence of the MXD spectrum, which consists of only two lines, the $2p_{3/2}$ and $2p_{1/2}$.

VI. INTEGRATED INTENSITY

As seen in Table IV the intensity decreases with the number of d electrons. The total intensity P of the transition $d^n\rightarrow 2p^5d^{n+1}$ summed over the three angular components of the dipole operator is equal to $(10-n)/5$, which is proportional to the number of holes and thus constant for a given d count.[34,35]

Without $3d$ spin-orbit splitting the L, Z, and R spectrum have the same integrated intensity. This can be seen in the low-spin configurations as well as in the $z=0$ configurations. With spin-orbit interaction the integrated intensities of the three dipole operator components are different. The difference is maximum in spherical symmetry. In the presence of a crystal field the spin-orbit interaction is partly quenched and the magnitude of $|P(l)-P(r)|$ is reduced. It decreases monotonically with the $3d$ spin-orbit interaction in going from O(3) to high-, intermediate-, and low-spin O_h field. This has the interesting consequence that the influence of the $3d$ spin-orbit interaction can be monitored by the integrated intensity of the $L-R$ spectrum. It provides a second way to determine the spin-orbit interaction, the other one is the value of the isotropic branching ratio.[26] The sign of the integrated $L-R$ spectrum depends on the number of $3d$ electrons. In O(3) symmetry ($10Dq=0$) the integrated intensity of the R spectrum is larger (smaller) than of the L spectrum for less (more) than half-filled shells. When there is no first-order spin-orbit splitting in O_h symmetry, the total intensities of the L, Z, and R spectra are the same, except for d^8 (O_h) where second-order spin-order interaction is important. In the presence of first-order spin-orbit splitting the total intensity of the R spectrum is larger (smaller) than that of the L spectrum, if the t_2 level is less (more) than half filled. Consequently, for low-spin configurations the integrated intensity of the $L-R$ spectrum is negative.

VII. BRANCHING RATIO

The branching ratio is the fraction of the total $2p$ line strength in the $2p_{3/2}$ manifold. The isotropic branching

ratio is the weighted sum of the branching ratio over the three dipole operator components, which is equal to the statistical value of $\frac{2}{3}$ when all final-state levels would be equally accessible. However, the accessibility of the final states is governed by the optical selection rules, and the branching ratio can deviate considerably from the statistical value. General rules for the *isotropic* branching ratio can be found in Ref. 26. Analysis of the anisotropic branching ratio is much more complex than in the isotropic case and will not be given here. Apart from $3d$ spin-orbit and $2p$-$3d$ interactions, there are other contributions which only depend on the symmetry of the ground state and the polarization of the light. Therefore, changes in the magnitude of the crystal-field parameters do not change the branching ratio, unless they change the symmetry of the ground state.

The spectra of the spin-orbit-split ground-state levels have a larger branching ratio than the spectra averaged over the spin-orbit split levels. This has been proven before[35] for the isotropic branching ratio, but it also seems to hold for the branching ratio of the separate polarized spectra. The values for the branching ratios of the various spectra are given in Table IV: As a rule of thumb, the branching ratio for the L spectrum is larger than for the R spectrum. There are only two exceptions: Cr d^4 ($t_2^3 e^1, {}^5E$) A_1 and Co $d^7 {}^4F_{9/2}$.

The configurations d^4 to d^7 have a spin transition when $10Dq$ is changed. The spectrum changes drastically because the new ground state selects another subset of final states. The low-spin state has a lower branching ratio than the high-spin state.[26]

Without spin-orbit splitting in O(3) and O_h (high-spin) symmetry, the difference in the branching ratio between the L and R spectra gradually increases along the series.

VIII. CONCLUSIONS

We have shown that a strong MXD effect is expected in the $2p$ edges of $3d$ transition-metal compounds due to the atomic dipole transitions between the $3d^n$ initial state and the $2p^5 3d^{n+1}$ final state. The branching ratio and integrated intensity show a systematic trend along the d series. In general, the branching ratio of the L spectrum

is larger than that of the R spectrum. The branching ratio depends on both the spin-orbit and exchange interactions. Characteristic values for the branching ratio have been given for each different ground-state symmetry (Table VI), which can be used to analyze experimental data. The branching ratio changes significantly in a high-spin to low-spin transition. The influence of the $3d$ spin-orbit splitting can be determined from the integrated intensity of the $L-R$ difference spectrum. In a material with spin-orbit interaction the integrated absorption for the two circular components of the x-ray radiation is different. This effect could be used to make a polarization filter or detector.

The exchange and spin-orbit interaction are both of the order of kT, which gives rise to a strong temperature and field dependence in the MXD spectra. Together with information from complementary magnetic techniques, such as susceptibility, Mössbauer, and paramagnetic resonance measurements, this can be used to determine the magnetic ground state.[22] MXD is ideally suited to measure magnetic overlayers and thin layers by using surface sensitive detection, such as electron yield and total reflection measurements. The spectra are very sensitive to minor changes in the exchange interaction. At room temperature the exchange interaction can even result in detectable changes in the isotropic spectrum due to mixing of higher J levels into the ground state.

The presented calculations are valid for compounds with localized $3d$ electrons, but further refinements might be needed to account for lower crystal-field symmetry, configuration interaction, and hybridization (mixing). Although in many cases the systematic trend obtained from the localized description will be a good approximation, we believe that for materials with delocalized valence electrons more theoretical work is necessary, especially for metallic magnetism, where the exchange interaction is much larger and band theory is a more suitable approach.

[1]P. M. Platzman and N. Tzoar, Phys. Rev. B **2**, 3356 (1970).

[2]F. deBergevin and M. Brunel, Phys. Lett. **39A**, 141 (1972).

[3]M. Blume, J. Appl. Phys. **57**, 3614 (1985); M. Blume and D. Gibbs, Phys. Rev. B **37**, 1779 (1988).

[4]J. P. Hannon, G. T. Tramell, M. Blume, and D. Gibbs, Phys. Rev. Lett. **61**, 1245 (1988).

[5]J. L. Erskine and E. A. Stern, Phys. Rev. B **12**, 5016 (1975).

[6]E. Keller and E. A. Stern, *EXAFS and Near Edge Structure III* (Springer, Berlin, 1984), p. 507.

[7]B. T. Thole, G. van der Laan, and G. A. Sawatzky, Phys. Rev. Lett. **55**, 2086 (1985).

[8]G. van der Laan, B. T. Thole, G. A. Sawatzky, J. B. Goedkoop, J. C. Fuggle, J. M. Esteva, R. Karnatak, J. P. Remeika, and H. A. Dabkowska, Phys. Rev. B **34**, 6529 (1986).

[9]J. B. Goedkoop, J. C. Fuggle, B. T. Thole, G. van der Laan, and G. A. Sawatzky, Nucl. Instrum. Meth. Phys. Res. A **273**, 429 (1988).

[10]H. Ebert, P. Strange, and B. L. Gyorffy, Z. Phys. B **73**, 77 (1988).

[11]G. Schütz, W. Wagner, W. Wilhelm, P. Kienle, R. Zeller, R. Frahm, and G. Materlik, Phys. Rev. Lett. **58**, 737 (1987).

[12]F. Baudelet, E. Dartyge, A. Fontaine, C. Brouder, G. Krill, J. P. Kapler, and M. Piecuch, Phys. Rev. B **43**, 5857 (1991).

[13]S. P. Collins, M. J. Cooper, A. Brahmia, D. Laundy, and T. Pitkanen, J. Phys. Condens. Matter **1**, 323 (1989).

[14]P. Carra and M. Altarelli, Phys. Rev. Lett. **64**, 1286 (1990).

[15]E. Beaurepaire, B. Carriere, and J. P. Kappler, *Rayonnement Synchrotron Polarisé, Electrons Polarisés et Magnétism*

(L'imprimé, Strasbourg, 1990).

[16]C. T. Chen and F. Sette, Rev. Sci. Instrum. **60**, 1616 (1989).

[17]C. T. Chen and F. Sette, Phys. Scr. T **31**, 119 (1990).

[18]C. T. Chen, F. Sette, Y. Ma, and S. Modesti, Phys. Rev. B **42**, 7262 (1990).

[19]F. Sette, C. T. Chen, Y. Ma, S. Modesti, and N. V. Smith, in *X-Ray and Inner-Shell Processes, Knoxville, 1990,* Proceedings of the 15th International Conference on X-Ray and Inner-Shell Processes, edited by T. A. Carlson, M. O. Krause, and S. T. Manson, AIP Conf. Proc. No. 215 (AIP, New York, 1990), p. 787.

[20]See, e.g., J. Zaanen, G. A. Sawatzky, and J. W. Allen, Phys. Rev. Lett. **55**, 418 (1985).

[21]T. Yamaguchi, S. Shibuya, S. Suga, and S. Shin, J. Phys. C **15**, 2641 (1982).

[22]G. van der Laan, B. T. Thole, G. A. Sawatzky, and M. Verdaguer, Phys. Rev. B **37**, 6587 (1988).

[23]B. T. Thole, G. van der Laan, and P. H. Butler, Chem. Phys. Lett. **149**, 295 (1988).

[24]F. M. E. de Groot, J. C. Fuggle, B. T. Thole, and G. A. Sawatzky, Phys. Rev. B **41**, 928 (1990).

[25]F. M. F. de Groot, J. C. Fuggle, B. T. Thole, and G. A. Sawatzky, Phys. Rev. B **42**, 5459 (1990). Their spectra for d^1, d^2, d^3, d^5, d^7 in the atomic case with zero crystal field contain errors which make them look different from the spectra with a small crystal field. The present paper contains the correct spectra.

[26]B. T. Thole, and G. van der Laan, Phys. Rev. B **38**, 3158 (1988).

[27]J. B. Goedkoop, J. C. Fuggle, B. T. Thole, G. van der Laan, and G. A. Sawatzky, J. Appl. Phys. **64**, 5595 (1988).

[28]J. B. Goodenough, Phys. Chem. Solids **6**, 287 (1958).

[29]J. Kanamori, Phys. Chem. Solids **10**, 87 (1959).

[30]P. H. Butler, *Point Group Symmetry, Applications, Methods and Tables* (Plenum, New York, 1981).

[31]R. D. Cowan, *The Theory of Atomic Structure and Spectra* (University of California Press, Berkeley, 1981).

[32]J. B. Goedkoop, B. T. Thole, G. van der Laan, G. A. Sawatzky, F. M. F. de Groot, and J. C. Fuggle, Phys. Rev. B **37**, 2086 (1988).

[33]G. van der Laan, Phys. Scr. **41**, 574 (1990).

[34]G. van der Laan and B. T. Thole, Phys. Rev. B **42**, 6670 (1990).

[35]B. T. Thole and G. van der Laan, Phys. Rev. A **38**, 1943 (1988).